

TRANSVERSE OSCILLATIONS DAMPING WITH WIDE-BAND FEEDBACK ON SPEAR II*

J. -L. Pellegrin

Stanford Linear Accelerator Center
Stanford University, Stanford, California 94306

Summary

With its high peak currents, SPEAR II is likely to show transverse coherent oscillations. A closed loop system using the beams as a signal path detects the bunches' center-of-mass motion and reacts on the beams after one machine period with a set of traveling wave electrodes. The detector senses oscillations at the betatron frequency and rejects signals due to equilibrium orbit shifts. The amplifier output is solely determined by the desired gain and the detector noise. Since, for a given machine tune, the system's phase margin can be made 90° by selecting the respective location of the pickup and feedback electrodes, stability is secured for all values of gain. However, one shows that critical damping cannot be obtained except with infinite gain, and that the system's damping rate is strictly equal to the gain per turn. Measurements of the loop gain have been carried out and agree with the observed damping. To date the system has been successful in dealing with injection oscillations and headtail instabilities.

1. Introduction

We describe a wide-band system in the sense that each bunch is considered as an independent oscillator with its own feedback loop; as a result all possible modes can be damped. For an observer standing at some point around the storage ring, the transverse motion of a beam looks similar to the sampled response of an oscillator. The pulses induced on an electrode constitute an amplitude modulated train with a carrier at the revolution frequency ω_0 , and a modulation at the frequency $(\nu-n)\omega_0$ where ν is the machine tune and n is an integer. For the purpose of the analysis the sampling can be ignored and the beam model becomes a continuous wave oscillator at the frequency $(\nu-n)\omega_0$; for shorter writing we take $n=0$. The Q of this oscillator depends mainly on the radiation losses, the chromaticity and the presence or absence of instabilities, but for the sake of our argument let us assume that the Q is relatively high and that the beam motion has a long damping time constant.

We have also to make all the assumptions required for the linearization of this model, that is small beam displacements, constant bunch length, no energy oscillations or current dependent instabilities, etc. The diagram of Fig. 1 shows the essential components of a loop: a wide-band power amplifier, a deflection electrode, the beam, a pickup

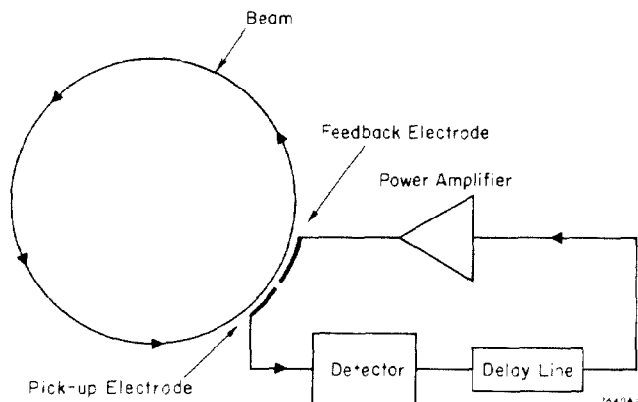


FIG. 1--Principle of the transverse beam feedback loop.

electrode, a beam position detector and a delay line. For a matter of convenience the pickup and feedback stations have been located at the same point on the machine, but for values of $\nu-n$ close to 0.25 or 0.75 they could as well be located any integer number of betatron half-wavelength apart.

We first turn to a description of the pickup and feedback electrodes and an evaluation of their main parameters.

2. Traveling Wave Electrodes

The sketch of Fig. 2 indicates the general disposition of a set of striplines as they are used to pick up the transverse

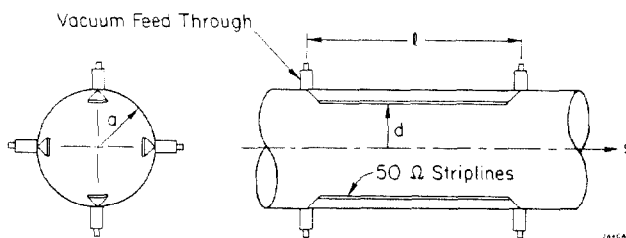


FIG. 2--Traveling wave electrode.

beam motion, or to excite the beams transversely. An analysis of this structure can be found in Ref. 1 where it is shown that such a pickup electrode can give a good reproduction of the time distribution of short beams. The photographs of Fig. 3 display the response of a 1 m electrode to

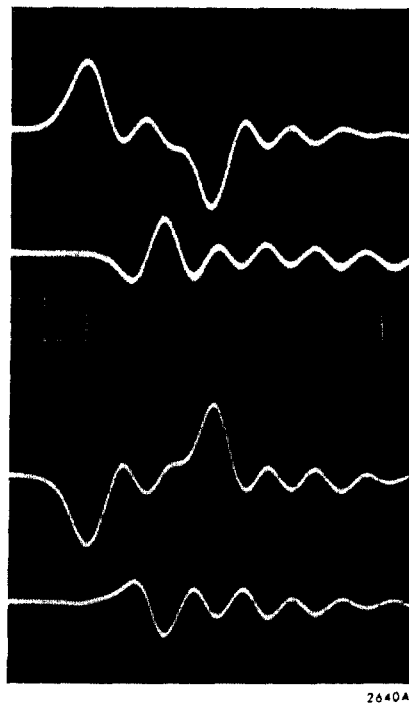


FIG. 3--Response of a 1 m electrode to 8 mA beams. The top two traces are the upstream and downstream signals induced by a positron beam, the bottom two traces are those of an electron beam. 10 volts/div, 2ns/div.

*Work supported by the U. S. Atomic Energy Commission.

8 mA beams; it is not representative of the bunch length because of the cable attenuation and the limited oscilloscope bandwidth (60 feet of $\frac{1}{2}$ in foam flex, and a 200 MHz oscilloscope), but it gives an indication of the directive properties of the strip* and yields a measurement for the current sensitivity S_c . For the actual setup and for a single electrode we get: $S_c = 2$ V peak/average mA.

a) Pickup Electrodes

One can express the output differential voltage v_p of a pair of electrodes in the following way:

$$v_p = \alpha \frac{2S_c}{a} i_{av} x_p \quad (1)$$

α is the attenuation of the cables; later on α will be taken as the attenuation of the complete detector. a in meter is a geometric factor analogous to the calibration factor of position monitors; it is approximately equal to the vacuum chamber radius; $a = 100$ mm. i_{av} is the average beam current in mA, and x_p in mm is a beam transverse displacement.

b) Deflection Electrodes

When a peak power P flows into one electrode (Fig. 2) in the s direction, the force exerted on a particle traveling in the $-s$ direction is given by:

$$F = 2\ell \sqrt{\eta P} k \quad (2)$$

where η is the impedance of free space and k in m^{-1} is a geometric factor for the electrode-vacuum chamber coaxial structure. For the case of a cylindrical rod in a cylindrical vacuum chamber, a value for k can be calculated from the electrostatic fields:

$$k = \frac{1}{4\pi} \sqrt{\frac{\eta}{Z_0}} \frac{2}{d} \left(1 + \frac{d^2}{a^2}\right) m^{-1} \quad (3)$$

d is the distance between the electrode center and the particle trajectory, a is the chamber radius and Z_0 is the electrode impedance:

$$Z_0 = \frac{\eta}{4\pi} \ln \left(\frac{d^2}{at} + \frac{d}{a} - \frac{a}{t} \right)^2 \quad (4)$$

with $2t$ the rod diameter.

For values of d/a close to unity, i.e., for low impedances, k does not depend very much on the shape of the electrode, and to a first order approximation we can use the plot of Eq. (3) (Fig. 4). It should be pointed out that these results apply also to cases where there is no net power flow (for instance when the electrode is open-ended and the current is momentarily zero). The force on a particle is due to the electric field only, which is then twice larger. One advantage is that deflection becomes identical for beams traveling in the $+s$ or $-s$ directions, whereas in the previous case, and for relativistic beams in particular, the $-s$ direction of propagation is essential to obtain a net force.

*On a laboratory model and with a bunch length of 1 ns, the directivity was of the order of 10. Here, the bunch length is probably 200 ps and the vacuum feedthroughs have a reflection coefficient of 0.2. This explains the rather poor directivity observed on Fig. 3.

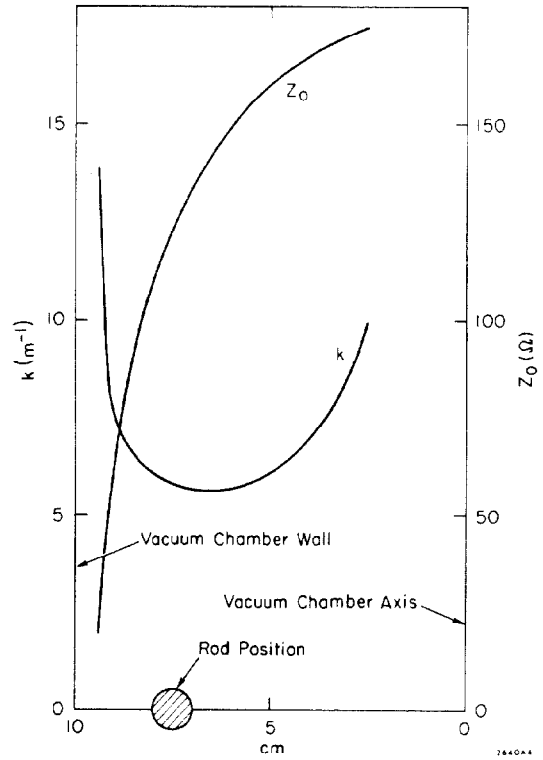


FIG. 4--Deflection coefficient and impedance of a cylindrical rod in a cylindrical vacuum chamber, with constant input power.

3. Transfer Function for the Beam Motion and Deflection System

The undamped harmonic motion of a particle excited by a deflection electrode of length ℓ , is described by the equation:

$$x_f + (\nu_0 \omega_0)^2 x_f = \frac{F(\nu_f) \omega_0 \ell}{2\pi p} \quad (5)$$

where x_f stands for a particle transverse position at the feedback electrode, and the driving term represents the time average force on a particle of momentum p . $F(\nu_f)$ is Eq. (2) in which P has been replaced by ν_f^2/Z_0 . Using s as the variable in the frequency domain we get:

$$\frac{X_f(s)}{V_f(s)} = 2e \sqrt{\frac{\eta}{Z_0}} \frac{k \omega_0 \ell}{2\pi p} \frac{1}{s^2 + (\nu_0 \omega_0)^2} \quad (6)$$

If now we pick x_f to be $\sin \nu \omega_0 t$, the beam motion at the pickup electrode will be $x_p = \sin \nu \omega_0 [t + (2\pi/\omega_0)]$ and will be a result of x_f . The Laplace transform of x_p/x_f yields the following transfer function:

$$\frac{X_p(s)}{X_f(s)} = \frac{\sin 2\pi\nu}{\nu \omega_0} \left(s + \frac{\nu \omega_0}{\tan 2\pi\nu} \right) \quad (7)$$

4. Closed Loop Linear Model

Relationships (1), (6) and (7) have been grouped in the block diagram of Fig. 5. Let us evaluate the system's open loop transfer function; we get:

$$K(s) = G \frac{\omega_0}{2\pi} \sin 2\pi\nu \frac{s + \frac{\nu \omega_0}{\tan 2\pi\nu}}{s^2 + (\nu_0 \omega_0)^2} \quad (8)$$

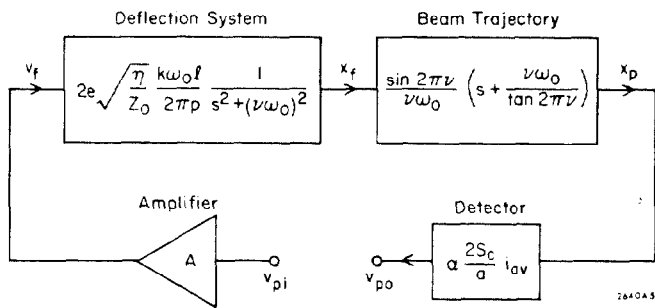


FIG. 5--Beam feedback loop transfer function; v_{pi} and v_{po} are used for open loop measurements.

with

$$G = 4 \sqrt{\frac{\eta}{Z_0}} \frac{k l c}{E \nu \omega_0} \alpha \frac{S_c}{a} i_{av} A$$

where A is the amplifier gain, E is the beam energy in eV and the other symbols are the same as in (1), (6) and (7). Stability and performance are best visualized when one plots the locus of the closed loop system poles as a function of the gain G. These poles are the complex roots of $1+K(s)$, and when their imaginary part is equated to $\nu\omega_0$, one obtains a relationship between G and ν which describes the locus:

$$\frac{1}{2} G \sin 2\pi\nu = \frac{2\pi\nu}{\tan 2\pi\nu} + 2\pi \sqrt{\left(\frac{\nu}{\tan 2\pi\nu}\right)^2 + \nu_0^2 - \nu^2} \quad (9)$$

The root locus is plotted on Fig. 6. For $G=0$ we have a pair of poles at $\pm(\nu_0-n)\omega_0^*$ and a zero at the origin. As G is increased, the closed loop poles describe the locus in the direction of the arrows; for a simple LC oscillator this locus would be a half circle intercepting the real axis at a finite value of G corresponding to critical damping. But here the zero moves toward infinity as G increases, and the locus becomes asymptotic to the negative real axis. As a result, critical damping is obtained for $G=\infty$ only, and it appears, in principle at least, that large loop gains should

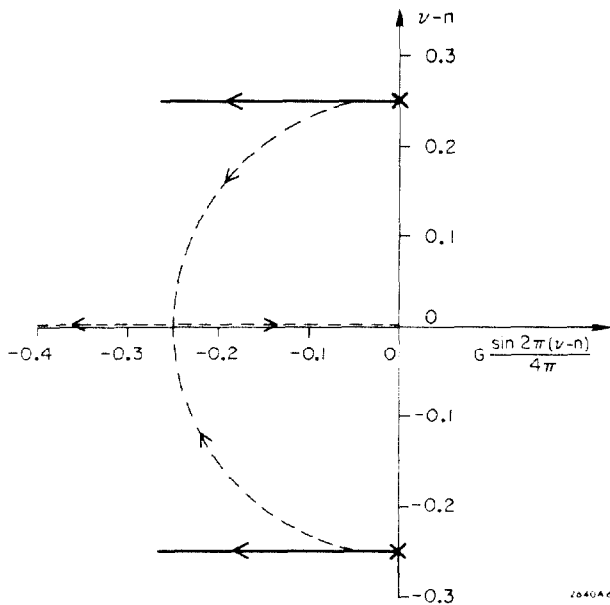


FIG. 6--Root locus of $1+K(s)$; the dotted line corresponds to the locus of a simple oscillator; both scales have to be multiplied by ω_0 .

*Figure 6 is plotted with $(\nu-n)$ instead of ν .

drive the beam to an integer resonance. However, since it is very difficult to achieve values of G larger than unity, this point has no practical consequence and the main interest of (9) is that it represents the closed loop system damping per turn, that is the damping rate is $(\omega_0/2\pi) G[\sin 2\pi(\nu-n)]/2$.

5. Detector Requirements and Circuit

The detector associated with a given bunch should perform the following functions:

- Produce a pulse train at the revolution frequency ω_0 having an amplitude modulation at $(\nu-n)\omega_0$.
- Gate out signals picked up from the motion of other bunches.
- Reject modulation components due to equilibrium orbit shifts, power supplies' ripple, synchrotron motion, bunch distortions, etc.

The circuit of Fig. 7 satisfies most of these requirements; its description can be found in more detail in Ref. 2. The

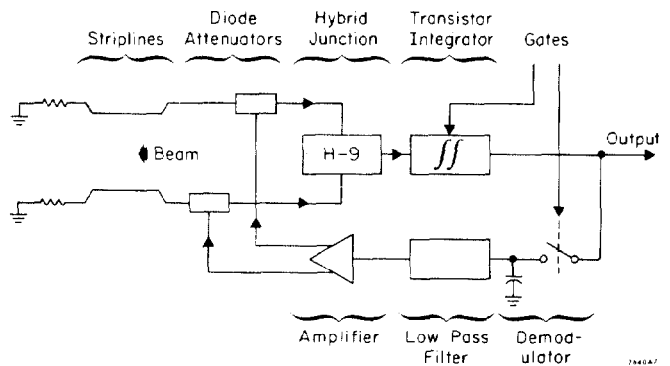


FIG. 7--Detector block diagram.

differential voltage of a pair of striplines is detected by a wide-band hybrid junction (Anzac H-9); the first integration of this pulse restores its dc component and the second gated integration yields a 30 ns pulse which is compatible with the power amplifier characteristics. A feedback loop consisting of a synchronous demodulator, a filter and an amplifier, reacts on two input diode attenuators. The forward response of this circuit is determined by the filter bandwidth. Figure 8 is a measurement of the relative output modulation amplitude as a function of frequency, for a beam of 8 mA. The input modulation was artificially produced by an oscillator connected to one of the control attenuators. The two curves corresponding to larger and smaller beam currents have been extrapolated from the measured curve.

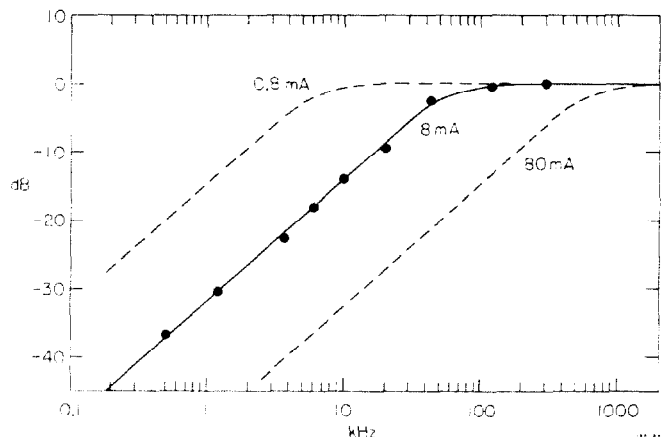


FIG. 8--Detector frequency response.

With the beams of SPEAR II the overall sensitivity of this detector has been found to be

$$v_p \approx 1.2 \cdot 10^{-3} i_{av}(\text{mA}) x_p(\text{mm}) \text{ volts} \quad (10)$$

and the residual noise attributed to finite hybrid junction isolation and gate feedthrough, is of the order of ± 5 mV; this is equivalent to beam orbit motions of ± 4 mA mm.

Figure 9 shows the detector output for a simulated 1 cm oscillation at 32 kHz and with a beam of 8 mA.

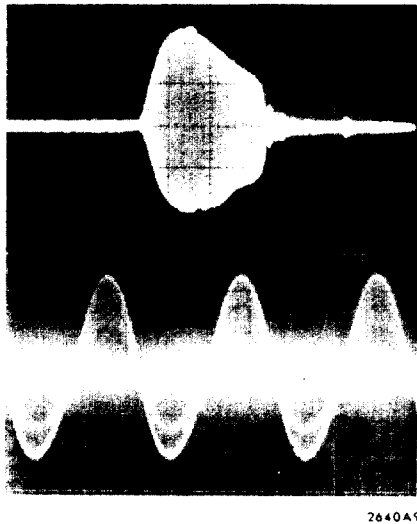


FIG. 9--Detector response to the simulated oscillation of an 8 mA beam. 50 mV/div; top 10 ns/div; bottom 10 μs/div.

To conclude we compare these results to the specification we set above and we find that the rejection of this circuit is adequate at low frequencies but quite insufficient at the synchrotron frequency. Indeed, we have a synchrotron frequency $\omega_s = 40$ kHz and we want to detect oscillations at $(\nu-n)\omega_0$ which extend from 100 to 300 kHz. The rejection of ω_s presents, for this wide-band circuit, a difficult problem which has not yet been solved.

6. Power Amplifier Output and Dynamic Range

It seems that a reasonable way for determining the power amplifier maximum output swing, would be to multiply the minimum detectable signal (here ± 5 mV) by the required amplifier gain, then to multiply by the dynamic range over which the system is to operate. So we should now proceed to calculate how much gain is needed to produce a given damping, but since, in the system design, we did not follow such a logical approach, let us return to the procedure that leads us to a practical solution.

A preliminary calculation indicated that an amplifier output of 500 volts into a 50 ohm electrode would produce the desired damping. So eight wide-band amplifiers comparable to the design of Ref. 3 were built and connected as shown on Fig. 10; they provide feedback for two beams in two dimensions, with pulses of up to 500 volts, 15 ns rise time and a maximum duty factor of 0.03.* The choice of the amplifier output swing and the measured detector residue impose now a maximum amplifier gain-dynamic range product of $500/5 \cdot 10^{-3} = 10^5$.

*After two years of operation the 4CX-250 tubes used in the output stage of these amplifiers have required an unusual amount of maintenance; a transistor design is presently under way.

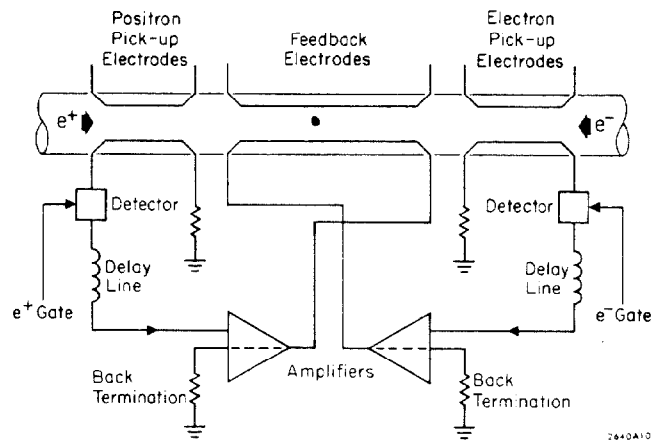


FIG. 10--Configuration of the e^+ and e^- loops.

7. Closed Loop Damping Rate of Linear System

From (8) one finds that the damping factor of $1+K(s)$ is $1/2 G(\omega_0/2\pi) \sin 2\pi\nu$. It turns out that for all practical values of G we have $\nu \approx \nu_0$ and assuming $\nu_0 \approx 5.25$ we write the damping time constant:

$$T_d = \frac{4\pi}{\omega_0 G} = \pi \sqrt{\frac{Z_0}{\eta}} \frac{E\nu_0}{k\ell c} \frac{a}{\alpha S_c} \frac{1}{i_{av} A} \quad (11)$$

with the following parameters: $Z_0=50$ ohms, $E=1.5 \cdot 10^9$ volts, $k=9 \text{ m}^{-1}$, $\ell=1$ m, $a=0.1$ m, $\alpha=30^{-1}$, $S_c=2$ volt/av mA we get:

$$T_d = \frac{5.0}{i_{av}(\text{mA}) A} \text{ sec} \quad (12)$$

This calculation neglects the beam natural damping which we hypothesized to be much longer than T_d .

For a 3.5 mA beam we have observed the waveform of Fig. 11 which represents the detected beam envelope during

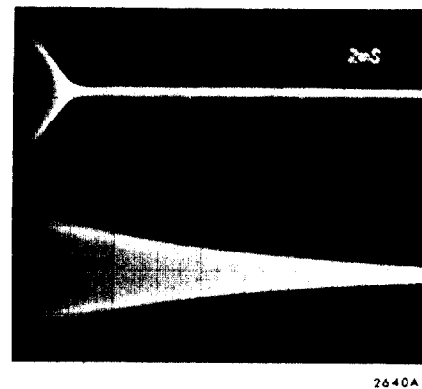


FIG. 11--Injected beam envelope, with and without feedback. Beam current 3.5 mA, chromaticity 0.5, 2ms/div.

an injection period (30 Hz repetition rate). The lower photograph is taken with no feedback and shows a damping time constant of 8 ms; the upper photograph represents the same envelope with feedback and a damping time constant which was minimized by adjusting the gain; saturation of the amplifier must indeed be avoided since, in effect, it decreases the loop gain. For $A=5000$ we measure a damping time constant of 1 ms, and from (12) we calculate $T_d=285 \mu\text{s}$.

So we conclude that within a factor of 3 this relationship can be used to figure the closed loop damping. The parameters which most likely are sources of error are k , S_c and α ; k cannot be measured, as for S_c and α they depend strongly on the bunch length.

Another test of this system capability consists in setting the storage ring with near zero chromaticity. With no feedback the injected beam cannot rise more than few milliamperes (typically 2 to 7 mA, for a chromaticity of 0), but with both vertical and horizontal feedback it becomes possible to inject up to 35 mA. Routine operation in this mode, or even with negative chromaticity, is contemplated for the future.

8. Conclusion

The design and operation of this wide-band damping system have been discussed. It applies in particular to a two-bunch storage ring. Since the damping rate of the linear model is approximately $\omega_0/4\pi G$, the specifications

require first of all a choice for the value of the loop gain G . The amplifier swing and gain can then be determined from the detector noise and sensitivity and from the desired dynamic range. On SPEAR II we have operated with amplifier gains between 5000 and 20,000, but we think that larger values would be desirable; so there does not seem to be any other alternative than building more powerful amplifiers and designing more efficient beam deflection systems.

Acknowledgment

It is a pleasure to thank Drs. B. Richter and J. McE. Paterson for promoting this system, and the SPEAR maintenance crew for keeping it operative.

References

1. Q. A. Kerns, D. B. Large, Lawrence Radiation Laboratory, Report No. UCRL-11551 (July 1964).
2. J. -L. Pellegrin, Nucl. Instr. and Methods 108, 365-373 (1973).
3. W. L. Gagnon and Bob H. Smith, IEEE Trans. Nucl. Sci. NS-16, 551 (1969).